ACS OMEGA

http://pubs.acs.org/journal/acsodf

Article

Application of Modified Smooth Exterior Scaling Method to Study $^2\Pi_g$ N_2^- and $^2\Pi$ CO^- Shape Resonances

Mwdansar Banuary and Ashish Kumar Gupta*

Cite This: *ACS Omega* 2023, 8, 7143−7150

Read Online

ACCESS | Metrics & More | Article Recommendations | Supporting Information

ABSTRACT: The modified smooth exterior scaling (MSES) method is applied for the first time to calculate the energy and the width of the electron-molecule scattering. The isoelectronic $^2\Pi_g$ N_2^- and $^2\Pi$ CO^- shape resonances have been studied as a test case for the MSES method. The results obtained using this method are in good agreement with experimental results. The conventional smooth exterior scaling (SES) method with different paths has also been applied for comparison purposes.

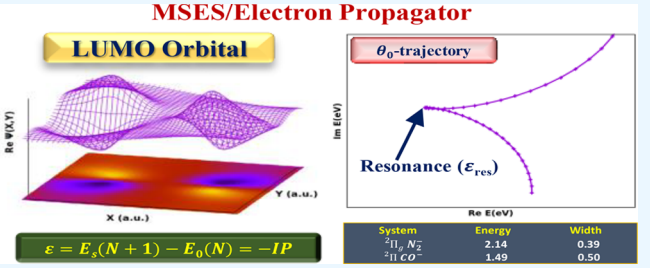

INTRODUCTION

Resonances are one of the most important phenomena in electron-molecule scattering. These are exponentially decaying long-lived metastable states of a system. These metastable states with a finite lifetime can break up into two or more subsystems.[1] These states can be considered as discrete states that are coupled to the continuum.[2] The first and most famous example, as well as application, was forwarded by Gamow[3] when he studied the α-decay of heavy nuclei in 1928. The resonances are complex eigenvalues of a Hamiltonian of the Schrodinger equation, which are characterized by $E_{res} = \varepsilon - i\Gamma/2$, where ε is the position of resonance and Γ is the width of the resonance or decay rate and is related to the lifetime of the metastable state (τ) by the relation $\tau = 1/\Gamma$. The resonance states in atomic and molecular systems are related to ionization potential (IP) and electron affinity (EA), which are calculated as the difference between the ground state total energies of the $(N \pm 1)$ and the neutral target that can be calculated using Koopman's theorem.[4]

In general, $IP = (E_s(N-1) - E_0(N)) = -\varepsilon_s$ and $EA = (E_0(N) - E_s(N+1)) = -\varepsilon_s$, where s labels a stationary state and $E_0(N)$ is the ground state total energy of the neutral N electron target, and the resonance energy and width are calculated as negative of IP and EA, i.e., ε_s, which are known as Auger and shape resonances, respectively. The corresponding resonance wave functions are not L^2-integrable. These wave functions diverge exponentially and therefore do not correspond to the Hermitian domain of the Hamiltonian owing to its asymptotic divergence behavior. Therefore, we have to convert the resonance wave functions into square integrable (part of Hilbert space) by using the proper transformation method. By carrying out a dilation transformation of the electronic coordinates, the resonance wave functions become square integrable. Mathematically, this transformation is the analytical continuation of Hamiltonian in the complex plane. This kind of scaling is known as the complex coordinate method or conventionally Complex Scaling (CS).[5−8]

The CS method has been widely applied in electronic resonances.[9−13] The CS method requires the potential part of the Hamiltonian to be an analytic function. Hence, this method cannot be applied to molecular systems within the Born−Oppenheimer approximation. Finally, Moiseyev and Corcoran[14] overcame such difficulty by carrying out analytical continuation of the Hamiltonian matrix elements.

The use of complex absorbing potential (CAP) was first introduced by Jolicard and co-workers.[15,16] Riss and Meyer[17,18] modified the basic concepts introduced by them. The motivation of applying CAP is very simple and obvious due to its simple implementation. Under the CAP method, the divergent resonance wave functions are converged into the physical domain of square integrable wave functions. When a wavepacket approaches the edge of a numerical grid artificial reflections occur and deteriorate the quality of the computed solution. The CAP is assumed to be zero in the interaction region and "turns on" where there are no interactions. In practice, the CAP attenuates the asymptotic part of the wavepacket and hence suppresses the artificial reflections. Due to its nonphysical nature, it generates artificial perturbations of the system which may cause a shift in the energy.[19]

Received: January 3, 2023
Accepted: February 1, 2023
Published: February 9, 2023

© 2023 The Authors. Published by American Chemical Society

A better alternative method to the CAP method is the smooth exterior scaling (SES) method.[20−25] SES is an efficient method based on the rigorous mathematical theory of CS to generate the wave functions without any artificial reflections at the grid boundary, and it does not disturb the interaction region. Hence, by applying SES similarity transformations to the Hamiltonian, a reflection-free complex absorbing potential is generated. Basically, the SES shares the property of CAP where the wavepacket is allowed to propagate along an arbitrary smooth path in the complex coordinate plane, and the wavepacket gets absorbed when the path leaves the real axis.

A modified smooth exterior scaling (MSES)[26,27] has been developed where the scaling path $[F(x)]$ is defined as $F(x) = xe^{i\theta} = xe^{i\theta(x)} = xe^{i\theta_0 a(x)}$, where $\theta(x)$ goes smoothly from 0 to θ_0 as $a(x)$ goes smoothly from 0 to 1. Instead, in SES, the derivative of the scaling path $[F(x)]$ is defined as $f(x) = \frac{\partial F}{\partial x} = 1 + [e^{i\theta_0} - 1]g(x)$, where θ_0 is the scaling parameter and $g(x)$ goes smoothly from 0 to 1, resulting in $f(x)$ going smoothly from 1 to $e^{i\theta_0}$. The scaling by the MSES method has been reported to be much smoother and displays efficient absorption during wavepacket propagation at the grid boundary.

Bivariational self-consistent field (SCF),[28,29] a complex scaled version of conventional SCF, had been implemented to study the resonance states in atomic[10,12,30,31] and molecular systems.[32−34] In this work, an attempt has been made to study the resonance states under the MSES. Hence, the method we are using here to study will be referred as bivariational SCF−MSES. The results obtained from bivariational SCF should improve by incorporating relaxation and correlation effects. So, to include these effects, the second order dilated (complex scaled by MSES) electron propagator (SoDEP−MSES) method is applied. The electron propagator theory[35] is a powerful tool in calculating electron detachment and attachment energies and correlated treatment of electronic structure. The dilated electron propagator[28] is proved as an effective and convenient method in characterizing Auger and shape resonances in atomic[10,30,36] and molecular systems.[37−39] This is the first time to use MSES method to study the shape resonances of molecular systems.

The paper is organized such that the next first section provides the theoretical background of MSES, bivariational SCF and the electron propagator. Then, results are shown and discussed along with two subsections, the $^2\Pi_g$ N_2^- shape resonance and the $^2\Pi$ CO^- shape resonance. Finally, conclusions are made with some future prospects and endeavor of the underlying methods.

THEORY

Modified Smooth Exterior Scaling (MSES). The SES has been discussed in detail in various publications.[20−25] For completeness, a brief introduction is included here. In SES, the scaling is done in the noninteraction region without affecting the interaction region and, hence, no scaling is required for the potential. The only difference between SES and MSES is that the scaling parameter $\theta(x)$ is complex in SES but is chosen as real in MSES.

The Moiseyev−Hirschfelder generalization[40] of the complex coordinate method associates the resonance poles of S-matrix, $E = E_r - iE_i$, with the θ_0 independent complex eigenvalues of $\hat{H}$:

$$\hat{H}\psi = E\psi \tag{1}$$

where

$$\hat{H} = -\frac{\hbar^2}{2M}\frac{\partial^2}{\partial z^2} + V(z) \tag{2}$$

Here, $z = F(x)$ is a path in the complex coordinate plane z, where

$$z = F(x) \to xe^{i\theta_0} \quad \text{as} \quad x \to \infty \tag{3}$$

The smooth-exterior path is defined as

$$f(x) = \frac{\partial F}{\partial x} = 1 + [e^{i\theta_0} - 1]g(x) \tag{4}$$

where $g(x)$ varies smoothly from 0 to 1 around the point $x = x_0$.

When $V(x \geq x_0) = 0$, then unscaled potential $V(x)$ can be used instead of complex potential $V(z)$. The corresponding transformed Hamiltonian $(\hat{H})$ has been derived in various publications.[20,22,25] It has the following form:

$$\hat{H} = \frac{-\hbar^2}{2M}\frac{\partial^2}{\partial x^2} + V[F(x)] + \hat{V}_{CAP} \tag{5}$$

where

$$\hat{V}_{CAP} = V_0(x) + V_1(x)\frac{\partial}{\partial x} + V_2(x)\frac{\partial^2}{\partial x^2} \tag{6}$$

and

$$V_0(x) = \frac{\hbar^2}{4Mf^3(x)}\frac{\partial^2 f(x)}{\partial x^2} - \frac{5\hbar^2}{8Mf^4(x)}\left(\frac{\partial f(x)}{\partial x}\right)^2 \tag{7}$$

$$V_1(x) = \frac{\hbar^2}{Mf^3(x)}\frac{\partial f(x)}{\partial x} \tag{8}$$

$$V_2(x) = \frac{\hbar^2}{2M}(1 - f^{-2}(x)) \tag{9}$$

Now, in the usual implementation of SES, the $g(x)$ [in eq 4] can be defined with the help of a certain family of integration paths in a complex coordinate plane, e.g.:[20,22]

$$g(x) = 1 + 0.5(\tanh(\lambda(x - x_0)) - \tanh(\lambda(x + x_0))) \tag{10}$$

SES following implementation using this method will be termed as conventional SES (CSES). The $F(x)$ can be derived by carrying out the integration over $g(x)$. Thus, the $F(x)$ will have the following form for the path given in the eq 10:

$$F(x) = x + (e^{i\theta} - 1)\left[x + \frac{1}{2\lambda}\ln\frac{\cosh[\lambda(x - x_0)]}{\cosh[\lambda(x + x_0)]}\right] \tag{11}$$

In CSES method, $g(x)$ is taken as real. Scaling function $\theta(x)$ and path $F(x)$ are related by the following relation:

$$F(x) = xe^{i\theta(x)} \tag{12}$$

As a result, $\theta(x)$ becomes complex.

In MSES, the scaling function $\theta(x)$ is chosen as real, which makes the $g(x)$ complex. The real function $\theta(x)$ is defined as

$$\theta(x) = a(x)\theta_0 = \theta \tag{13}$$

where θ_0 is the scaling parameter and $a(x)$ is chosen as follows:

https://doi.org/10.1021/acsomega.3c00033
ACS Omega 2023, 8, 7143−7150

$$a(x) = 1 + 0.5(\tanh(\lambda(x - x_0)) - \tanh(\lambda(x + x_0))) \quad (14)$$

The value of $a(x)$ varies from 0 to 1 around the point $x = x_0$. The corresponding path will be defined as

$$F(x) = xe^{i\theta(x)} \quad (15)$$

and the $g(x)$ related to MSES path will have the following form:[26]

$$g(x) = \frac{e^{i\theta} - 1}{e^{i\theta_0} - 1} + ix\frac{e^{i\theta}}{e^{i\theta_0} - 1}\theta_0\lambda\, 0.5[\sec h^2(\lambda(x - x_0)) - \sec h^2(\lambda(x + x_0))] \quad (16)$$

There are several other existing paths that can be chosen for the calculations. We are using the following paths in our investigation along with MSES path:

Path-I[20,25]

$$g(x) = 1 + 0.5(\tanh(\lambda(x - x_0)) - \tanh(\lambda(x + x_0))) \quad (17)$$

$$F(x) = x + (e^{i\theta} - 1)\left[x + \frac{1}{2\lambda}\ln\frac{\cosh[\lambda(x - x_0)]}{\cosh[\lambda(x + x_0)]}\right] \quad (18)$$

Path-II[20,25]

$$g(x) = (1 + e^{(x_0 - x)\lambda})^{-1} + (1 + e^{(x_0 + x)\lambda})^{-1} \quad (19)$$

$$F(x) = x + (e^{i\theta} - 1)\left[2x - \frac{1}{\lambda}\ln\left(1 + e^{(x_0 + x)\lambda}\right) + \frac{1}{\lambda}\ln\left(1 + e^{(x_0 - x)\lambda}\right)\right] \quad (20)$$

Path-III[23,25]

$$g(x) = \begin{cases} 0, & x \le x_0 \\ 1 - e^{-\lambda(x - x_0)^2} + 2\lambda(x - x_0)^2 e^{-\lambda(x - x_0)^2}, & x > x_0 \end{cases} \quad (21)$$

$$F(x) = \begin{cases} x, & x \le x_0 \\ x + (e^{i\theta} - 1)(x - x_0)(1 - e^{-\lambda(x - x_0)^2}), & x > x_0 \end{cases} \quad (22)$$

Bivariational SCF. In the complex SCF method (also known as bivariational SCF),[28,29] the dilated Hamiltonian is used along with real basis functions. Here, the complex scaled Hamiltonian $H(\eta)$, where $\eta = xe^{i\theta}$ loses the properties of Hermitian and becomes non-Hermitian, i.e., $H^\dagger(\eta) = H^*(\eta) \neq H(\eta)$. Therefore, variational theorem becomes inapplicable. However, a bivariational theorem is applicable for complex symmetric operators. To apply the bivariational method, the functional

$$E(\Phi_0\Psi_0) = \frac{\langle\Phi_0|H(\eta)|\Psi_0\rangle}{\langle\Phi_0|\Psi_0\rangle} \quad (23)$$

is extremized to obtain the bivariational SCF equations with conditions Φ_0 and Ψ_0 should be single determinants

$$\Phi_0 = (N!)^{-1/2}\det\{\phi_i(x_i)\} \quad (24)$$

$$\Psi_0 = (N!)^{-1/2}\det\{\psi_j(x_j)\} \quad (25)$$

where $i = j = 1, 2, ..., N$ and the constituent one-electron orbitals ϕ and ψ should be biorthonormal

$$\langle\phi_i|\psi_j\rangle = \delta_{ij} \quad (26)$$

The following SCF equations can be obtained by extremizing the functional eq 23

$$\Omega\phi_i = \epsilon_i\phi_i \quad (27)$$

$$\Omega^+\psi_i = \epsilon_i^*\psi_i \quad (28)$$

where

$$\Omega_1(\eta, \phi, \psi) = -\frac{1}{2}\eta^2\Delta_1^2 - \eta\frac{Z}{r_1} + \eta\int_{x_{2'}=x_2}\frac{1 - P_{12}}{r_{12}}\rho(x_{2'}, x_2)\, dx_2 \quad (29)$$

with

$$\rho = \sum_i^{occ}\phi_i\psi_i^* \quad (30)$$

The dilated Hamiltonian is complex symmetric, i.e, $H^\dagger(\eta) = H^*(\eta)$. Since the choice of basis function has the property as $\Phi = \Psi^*$, the many-electron wave function satisfies the same relation. The detailed implementation and the advantages of bivariational SCF is described in ref.[29]

However, in the case of SES, only the outer region is scaled, and hence the Fock operator for a molecule takes the form as follow:

$$\Omega_1(\eta, \phi, \psi) = -\frac{1}{2}\Delta_1^2 - \sum_A\frac{Z_A}{r_{1A}} + \int_{x_{2'}=x_2}\frac{(1 - P_{12})}{r_{12}}\rho(x_{2'}, x_2)\, dx_2 + \hat{V}_{CAP}(r_1) \quad (31)$$

where

$$\hat{V}_{CAP}(r) = \hat{V}_{CAP}(x) + \hat{V}_{CAP}(y) + \hat{V}_{CAP}(z) \quad (32)$$

and $\hat{V}_{CAP}(x)$ is defined in eq 6.

To evaluate

$$\langle p(x, y, z)|\hat{V}_{CAP}(x)|q(x, y, z)\rangle \quad (33)$$

where $p(x, y, z)$ and $q(x, y, z)$ are primitive Gaussian basis, defined as

$$p(x, y, z) = N_p x^l y^m z^n\, e^{-\alpha(r - r_0)^2} \quad (34)$$

and centered at $r_0 = (x_0, y_0, z_0)$.

$p(x, y, z)$ can be written as

$$p(x, y, z) = N_p p_x p_y p_z \quad (35)$$

where $p_x = x^l\, e^{-\alpha(x - x_0)^2}$ and similarly p_y and p_z. Hence, the expression (33) can be partitioned as

$$N_p N_q\langle p_x p_y p_z|\hat{V}_{CAP}(x)|q_x q_y q_z\rangle = N_p N_q\langle p_x|\hat{V}_{CAP}(x)|q_x\rangle\langle p_y|q_y\rangle\langle p_z|q_z\rangle \quad (36)$$

where $\langle p_y|q_y\rangle$ and $\langle p_z|q_z\rangle$ are evaluated analytically and $\langle p_x|\hat{V}_{CAP}(x)|q_x\rangle$ being a one-dimensional integral is evaluated numerically.

https://doi.org/10.1021/acsomega.3c00033
ACS Omega 2023, 8, 7143−7150

The Electron Propagator. The electron propagator theory is considered an efficient method in improving the electron affinities and ionization potentials that are calculated from the bivariational SCF level. These improvements can be done by introducing an effective potential, called self-energy, which was formulated by Dyson.[4] The Dyson equation for dilated electron propagator **G** can be written as[38]

$$\mathbf{G}(\eta, E) = \mathbf{G}_0(\eta, E) + \mathbf{G}_0(\eta, E)\Sigma(\eta, E)\mathbf{G}(\eta, E) \tag{37}$$

where $\mathbf{G}_0(\eta, E)$ is known as the zeroth order dilated electron propagator and is a matrix of the electron propagator of uncorrelated electron motion and $\Sigma(\eta, E)$ is defined as

$$\Sigma(\eta, E) = \Sigma^{(2)}(\eta, E) + \Sigma^{(3)}(\eta, E) + ... \tag{38}$$

$\Sigma(\eta, E)$ is the matrix representation of the exact self-energy in the basis of spin orbitals which is the sum of different orders such as second order, $\Sigma^{(2)}(\eta, E)$, and third order, $\Sigma^{(3)}(\eta, E)$. This self-energy matrix contains the relaxation and correlation effects.

In particular, the elements of the second order self-energy matrix are given as follows[4,35]

$$\Sigma_{ij}^{(2)}(\eta, E) = \frac{1}{2}\Sigma_{ars}\frac{\langle rs||ia\rangle\langle ja||rs\rangle}{E(\eta) + \epsilon_a(\eta) - \epsilon_r(\eta) - \epsilon_s(\eta)} + \frac{1}{2}\Sigma_{abr}\frac{\langle ab||ir\rangle\langle jr||ab\rangle}{E(\eta) + \epsilon_r(\eta) - \epsilon_a(\eta) - \epsilon_b(\eta)} \tag{39}$$

where the indices *a*, *b*, ... represent occupied spin orbitals, *r*, *s*, ... represent unoccupied spin orbitals, and *i*, *j*, ... represent unspecified orbitals, and the antisymmetric two-electron integral is given by

$$\langle ij||kl\rangle = \eta^{-1}\int \psi_i(1)\psi_j(2)\frac{(1 - P_{12})}{r_{12}}\psi_k(1)\psi_l(2)\, dx_1\, dx_2 \tag{40}$$

To calculate the lowest order correction, we are ignoring the off-diagonal elements of self-energy ($\Sigma(\eta, E)$).[4,35] Consequently, the associated pole search becomes easy just by solving the following equation

$$E(\eta) = \epsilon(\eta) + \Sigma_{ii}(\eta, E) \tag{41}$$

where E is an electron binding energy. The solution can be done repeatedly starting with $E = \epsilon_i$ until the convergence result is found. The lowest-order correction with second order self-energy to ϵ_i is given by the following equation

$$\epsilon_i' = \epsilon_i + \Sigma_{ii}^{(2)}(\epsilon_i) \tag{42}$$

RESULTS AND DISCUSSION

The isoelectronic systems $^2\Pi_g$ N_2^- and $^2\Pi$ CO^- have been the prototypical systems used to test the effectiveness of new theoretical methods to treat the molecular shape resonances. We apply the bivariational SCF−MSES and SoDEP−MSES methods to study the molecular shape resonances. We are testing the efficacy of the MSES method using the mentioned systems. Atomic units are used throughout unless otherwise stated. The basis set we employed to study the $^2\Pi_g$ N_2^- and $^2\Pi$ CO^- shape resonances is aug-cc-pCVDZ with augmentation. The basis set for all the atoms are augmented for the accommodation of an electron of the metastable state. The most diffused functions of type s and p are augmented by multiplying the factor of $\frac{1}{2^n}$ for n = 1, 2, ..., 5. Hence, the augmented basis functions will be referred to as aug-cc-pCVDZ+5s5p(A).

Resonances are generally the stationary points obtained through stable point search in θ_0-trajectories of complex orbital energies following the complex virial theorem.[41] The stability of the resonance energy is obtained through the relation

$$\frac{\partial E}{\partial \eta} = 0 \tag{43}$$

where $\eta = xe^{i\theta_0 a(x)}$ and $a(x)$ is associated with parameters x_0 and λ. Equivalently, the optimum approximate resonance eigenvalue follows:

$$\left(\frac{\partial E}{\partial \theta_0}\right)_{\lambda_{\text{optimum}}, x_{0\text{optimum}}} = 0 \tag{44}$$

In practice, the above complex virial theorem leads to cusps, loops, or kinks or slows down at the poles obtained in the θ_0-trajectories.

The MSES method generally depends on several parameters, λ, x_0, and θ_0. Each one of these parameters is associated with a stabilization point (cusp) in a plot when the resonance energy is plotted as a function of θ_0, keeping other parameters fixed. The cusp so obtained represents a resonance state. We have performed a series of calculations for various x_0 and λ parameters, and the value of parameter λ is chosen as 10.0 au from the set of well-stabilized resonance θ_0-trajectories. The same value of λ is also applied by Y. Sajeev et al. to study the Feshbach type autoionization resonance of a helium atom[42] and hydrogen molecule.[43] The corresponding θ_0-trajectories have been plotted using the respective x_0 values for the $^2\Pi_g$ N_2^- and $^2\Pi$ CO^- shape resonances.

The $^2\Pi_g$ N_2^- Shape Resonance. The $^2\Pi_g$ N_2^- shape resonance is perhaps the most studied molecular resonance among electron-molecule scattering problems studied so far. The basis set aug-cc-pCVDZ+5s5p(A) is employed for each nitrogen atom. The N_2 molecule is placed along the *x*-axis symmetrical to the origin considering the bond length of 1.09 Å. For the bivariational SCF−MSES method, the θ_0-trajectories using different complex scaling paths, i.e. MSES Path, Path-I, Path-II and Path-III, are plotted in Figure 1. Same values of different parameters are used for all the paths (λ = 10.0 and x_0 = 4.5). We have not added any dc field[42,43] to the Hamiltonian either in CSES or in MSES. In the figure, no clear stationary points (i.e., cups or kinks) are observed except for MSES path.

In Figure 1, in the case of MSES path, there are many closely spaced curves which contain kinks or stationary points. Out of many kinks shown in the figure, only one of them represents the $^2\Pi_g$ N_2^- shape resonance, which is shown by an arrow. Others are artifacts due to an incomplete basis set. Whether a state is a resonance or artifact can be identified by plotting the orbital wave function.[44] A resonance state is localized within the interaction region, but a continuum or artifacts will be localized outside the interaction region. As the SES does not affect the interaction region, the shape of molecular orbitals in the interaction region do not get distorted much. Therefore, we have plotted the molecular orbitals at the stationary point to check which curve belongs to the π_g* state. The orbital corresponding to that state is plotted in Figure 2, which shows a typical π_g* character of the lowest unoccupied molecular orbital (LUMO). Only the real part of the orbital is plotted, as

https://doi.org/10.1021/acsomega.3c00033
ACS Omega 2023, 8, 7143−7150

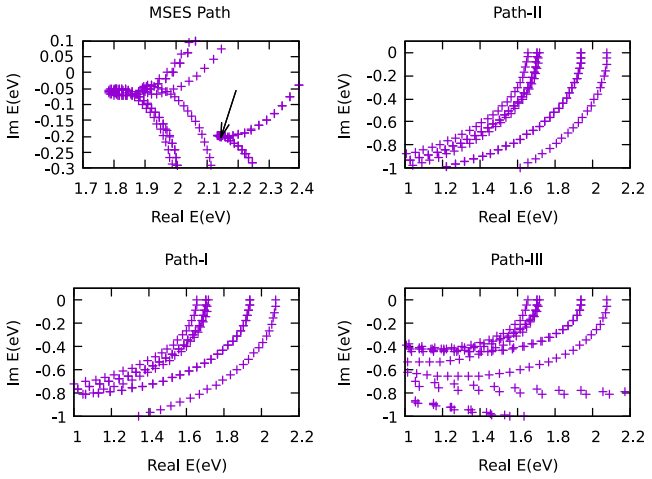

Figure 1. θ_0-trajectories of orbital energies of N_2 for x_0 = 4.5 using MSES Path, Path-I, Path-II, and Path-III. Cusps are seen only for MSES path. The arrow shows the position of the $^2\Pi_g$ N_2^- shape resonance. Other cusps are artifacts as concluded after plotting orbitals.

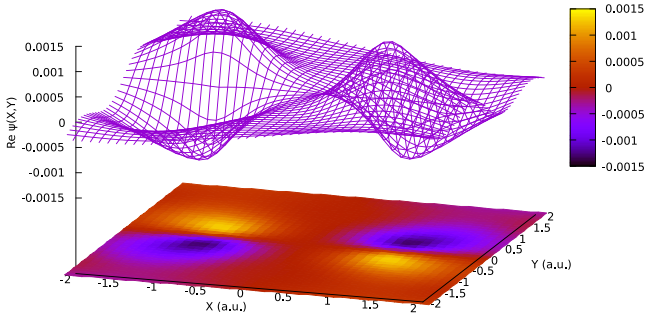

Figure 2. Resonance wave function of the $^2\Pi_g$ N_2^- shape resonance. The positions of two N atoms are at 0.545 and −0.545 along the x-axis.

the imaginary part is an order smaller than the real part. If the absolute value of the wave function is plotted, then the nodal structure will be lost. The corresponding resonant-θ_0-trajectory is displayed in Figure 3. The optimal θ_0 value at the stationary point is 0.24. The values of energy and width obtained from the real and imaginary part of the resonant pole are 2.14 and 0.39 eV, respectively.

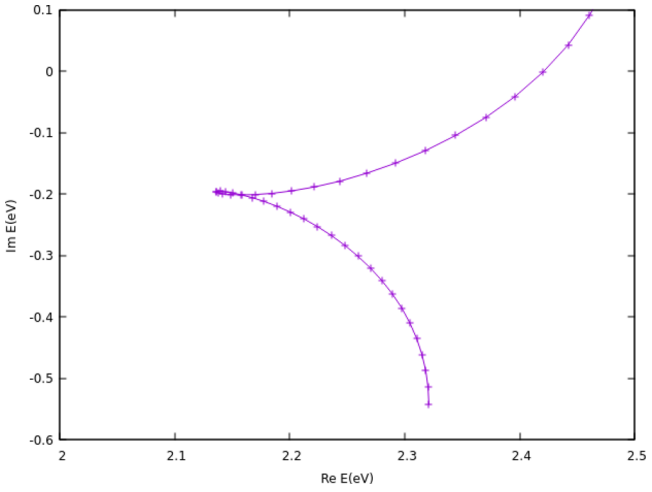

Figure 3. θ_0-trajectory of the $^2\Pi_g$ N_2^- shape resonance at x_0 = 4.5 using vivariational SCF−MSES.

The SoDEP−MSES method is employed to improve the results obtained from the bivariational SCF level. The resonant-θ_0-trajectory for SoDEP−MSES is given in Figure 4.

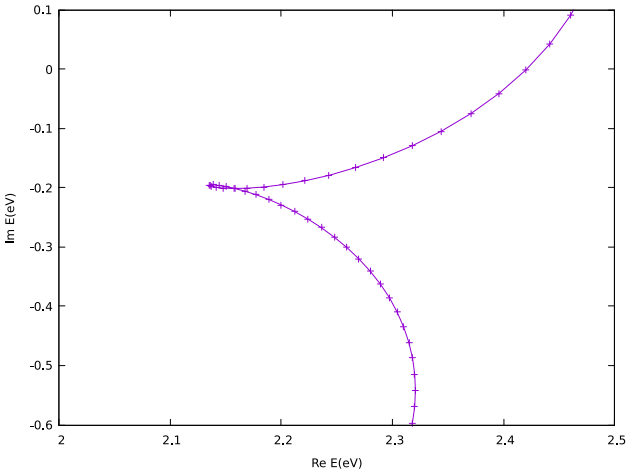

Figure 4. θ_0-trajectory of $^2\Pi_g$ N_2^- shape resonance at x_0 = 4.5 using SoDEP−MSES.

The results obtained from both bivariational SCF−MSES and SoDEP−MSES methods show no discernible difference. S. Mahalakshmi et al.[39] also reported no considerable change while performing a higher-order dilated electron propagator to the $^2\Pi_g$ N_2^- shape resonance. The same conclusion can be drawn from this work. McCurdy et al.[44] also indicated that some well-known molecular shape resonances (N_2^-, CO^-, F_2^-, etc.) can be characterized at the bivariational SCF level itself. The energy and width obtained from the bivariational SCF−MSES and SoDEP−MSES methods along with other theoretical methods and experiment results are collected in Table 1. As compared to other theoretically calculated results, the results obtained from bivariational SCF−MSES and SoDEP−MSES methods are in good agreement with experimental results.

The $^2\Pi$ CO^- Shape Resonance. The basis set employed to investigate $^2\Pi$ CO^- shape resonance is aug-cc-pCVDZ +5s5p(A) centered on C and another aug-cc-pCVDZ+5s5p(A) centered on O. The CO molecule is set along the x-axis symmetrical to the origin considering the bond length 1.128 Å. For the bivariational SCF−MSES method, using the same values of different parameters (λ = 10.0, x_0 = 3.3), θ_0-trajectories for four different paths (i.e., MSES path, Path-I, Path-II, and Path-III) are plotted as displayed in Figure 5 without adding any dc field to the Hamiltonian.

In Figure 5, no clear stationary points are observed except for the MSES path. So, in the MSES path, to confirm which curve belongs to the $^2\Pi$ state, we have plotted the molecular orbitals at the stationary points. The orbital corresponding to that state is plotted in Figure 6, which is a π^* LUMO with greater amplitude on the carbon atom.[39] As in the case of the $^2\Pi_g$ N_2^- shape resonance, we have plotted only the real parts of the orbital. The corresponding resonant-θ_0-trajectory has been plotted in Figure 7. The value of the resonance energy and width obtained from this work along with other theoretical methods and experimental results are displayed in Table 2. We

https://doi.org/10.1021/acsomega.3c00033
ACS Omega 2023, 8, 7143−7150

Table 1. Energy and Width of the $^2\Pi_g$ N_2^- Shape Resonance

Method	Energy (eV)	Width (eV)
Experiment[45]	2.32	0.41
Linear algebra method[46]	2.13	0.31
Static exchange R-matrix[47]	2.15	0.34
Stabilization method[48]	2.44	0.32
Boomerang model[49]	1.91	0.54
Complex SCF[50]	3.19	0.44
Second order dilated electron propagator (real SCF)[51]	2.14	0.26
CAP−FSMRCC[52]	2.52	0.39
dp−CAP−EOM−EA−CCSD ($r_j^{CAP} \neq 0$)[53]	2.75	0.26
rm−CAP−EOM−EA−CCSD ($r_j^{CAP} \neq 0$)[54]	2.50	0.35
rm−CAP−EOM−EA−CCSD ($r_j^{CAP} = 0$)[54]	2.53	0.32
EOM−EA−CCSD[55]	2.54	0.52
MCSCF−CAP[56]	3.12	0.31
CAP/EA−ADC(3)[57]	2.54	0.40
CAP/PP−CASSCF[58]	3.83	0.25
Results from biorthogonal dilated electron propagator[39]		
Zeroth order, quasi particle second order, and quasi particle diagonal 2ph−TDA	2.12	0.19
Second order	2.11	0.18
Diagonal 2ph−TDA	2.12	0.18
Quasi-particle/OVGF third order	2.11	0.18
Third order	2.11	0.18
Bivariational SCF−MSES (This work)	2.14	0.39
SoDEP−MSES (This work)	2.14	0.39

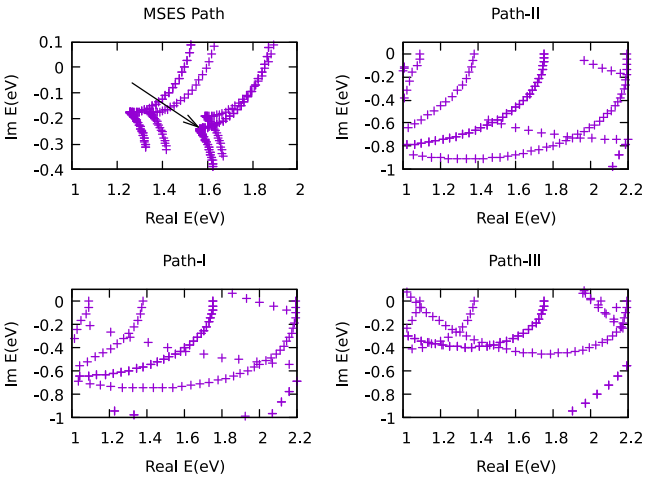

Figure 5. θ_0-trajectories of orbital energies of CO for x_0 = 3.3 using MSES Path, Path-I, Path-II, and Path-III. Cusps are seen only for MSES path. The arrow shows the position of the $^2\Pi$ CO^- shape resonance. Other cusps are artifacts as concluded after plotting orbitals.

would like to mention that the energy and width that are obtained in our calculation are 1.57 and 0.49 eV, respectively. The reported optimal values of θ_0 is 0.34 at the stationary point. As in the case of the $^2\Pi_g$ N_2^- shape resonance, here also SoDEP−MSES is applied. The resonant-θ_0-trajectory for the SoDEP−MSES method is displayed in Figure 8. The resonance position obtained from the SoDEP−MSES method shows improvement. However, the results obtained from both the bivariational SCF−MSES and SoDEP−MSES methods are very close to the experimental results and in good agreement with the other results that are obtained from various theoretical methods.

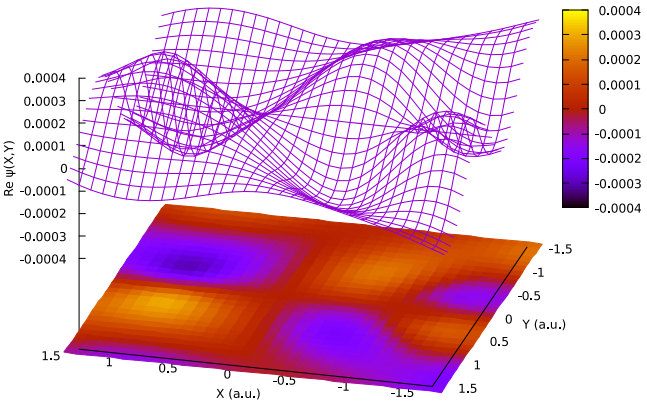

Figure 6. The resonance wave function of the $^2\Pi$ CO^- shape resonance. The positions of C and O atoms are at 0.564 and −0.564 along x-axis, respectively.

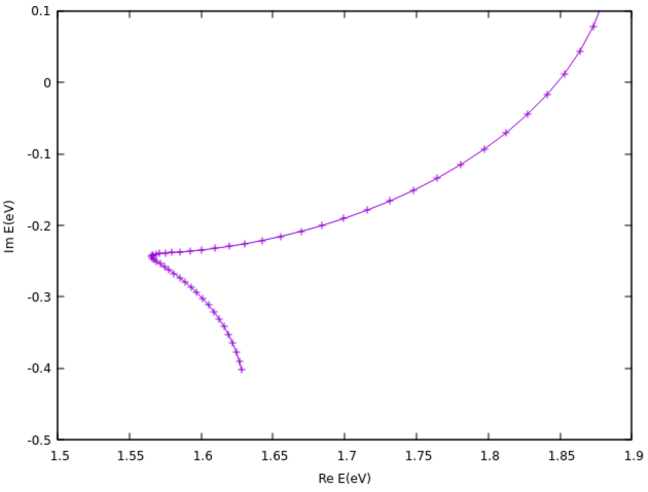

Figure 7. θ_0-trajectory of the $^2\Pi$ CO^- shape resonance at x_0 = 3.3 using bivariational SCF−MSES.

Table 2. Energy and Width of the $^2\Pi$ CO^- Shape Resonance

Method	Energy (eV)	Width (eV)
Experiment[59]	1.50	0.40
Boomerang model[60]	1.52	0.80
Close coupling method[61]	1.75	0.28
Second order dilated electron propagator (real SCF)[62]	1.71	0.10
dp−CAP−EOM−EA−CCSD ($r_j^{CAP} \neq 0$)[53]	1.98	0.59
rm−CAP−EOM−EA−CCSD ($r_j^{CAP} \neq 0$)[54]	2.01	0.60
rm−CAP−EOM−EA−CCSD ($r_j^{CAP} = 0$)[54]	2.09	0.61
EOM−EA−CCSD[55]	2.04	1.03
MCSCF−CAP[56]	1.28	0.32
CAP/EA−ADC(3)[57]	1.95	0.63
CAP/PP−CASSCF[58]	2.16	0.31
Results from biorthogonal dilated electron propagator[39]		
Zeroth order, quasiparticle second order and quasiparticle diagonal 2ph-TDA	1.71	0.10
Second order	1.68	0.09
Diagonal 2ph-TDA	1.69	0.08
Quasi-particle third order and OVGF third order	1.65	0.14
Third order	1.65	0.14
Bivariational SCF−MSES (This work)	1.57	0.49
SoDEP−MSES (This work)	1.49	0.50

https://doi.org/10.1021/acsomega.3c00033
ACS Omega 2023, 8, 7143−7150

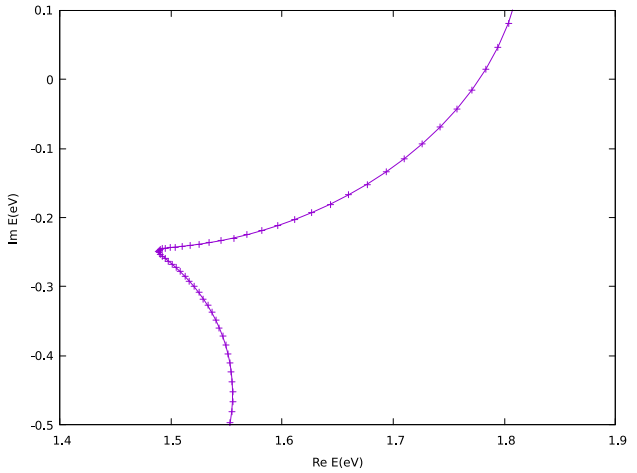

Figure 8. θ_0-trajectory of the $^2\Pi$ CO^- shape resonance at x_0 = 3.3 using SoDEP−MSES.

CONCLUSIONS

In this paper, the bivariational SCF−MSES and SoDEP−MSES methods have been applied for the first time to study the shape resonances in electron-molecule scattering. The $^2\Pi_g$ N_2^- and $^2\Pi$ CO^- shape resonances have been studied. The results obtained in this work using the MSES method compare well with experimental results. Also, we perform a comparison with different complex scaling paths. It is clear that conventional SES can not be used as-is to study the shape resonance. From this work, it is also observed that the bivariational SCF−MSES and SoDEP−MSES methods give better results than calculations done using other methods. Therefore, we can conclude that the MSES method is quite reliable and effective to investigate molecular shape resonances.

ASSOCIATED CONTENT

Supporting Information

The Supporting Information is available free of charge at https://pubs.acs.org/doi/10.1021/acsomega.3c00033.

Plots of wave functions of artifacts as seen in θ_0-trajectories (PDF)

AUTHOR INFORMATION

Corresponding Author

Ashish Kumar Gupta − *Department of Chemistry, Indian Institute of Technology, Guwahati 781039 Assam, India;* orcid.org/0000-0003-0054-0093; Phone: 0361 258 2312; Email: gupta@iitg.ac.in; Fax: 0361 258 2349

Author

Mwdansar Banuary − *Department of Chemistry, Indian Institute of Technology, Guwahati 781039 Assam, India*

Complete contact information is available at: https://pubs.acs.org/10.1021/acsomega.3c00033

Notes

The authors declare no competing financial interest.

ACKNOWLEDGMENTS

The authors would like to acknowledge the PARAM−ISHAN supercomputing centre in IIT Guwahati for providing us with high performance computing facility. This study was supported in part by a research grant from the Department of Science and Technology, New Delhi, India (DST Grant No. SB/S1/PC−82/2012). M.B. is thankful to MHRD, India for research fellowship.

REFERENCES

(1) Moiseyev, N. *Non-Hermitian Quantum Mechanics*; Cambridge University Press, 2011.
(2) Klaiman, S.; Gilary, I. *Adv. Quantum Chem.*; Elsevier, 2012; Vol. *63*; pp 1−31.
(3) Gamow, G. Quantum theory of the atomic nucleus. *Z. Phys.* **1928**, *51*, 204−212.
(4) Szabo, A.; Ostlund, N. S. *Modern Quantum Chemistry: Introduction to Advanced Electronic Structure Theory*; Courier Corporation, 2012.
(5) Aguilar, J.; Combes, J.-M. A class of analytic perturbations for one-body Schrödinger Hamiltonians. *Commun. Math. Phys.* **1971**, *22*, 269−279.
(6) Balslev, E.; Combes, J.-M. Spectral properties of many-body Schrödinger operators with dilatation-analytic interactions. *Commun. Math. Phys.* **1971**, *22*, 280−294.
(7) Simons, J. The complex coordinate rotation method and exterior scaling: A simple example. *Int. J. Quantum Chem.* **1980**, *18*, 113−121.
(8) Reinhardt, W. P. Complex coordinates in the theory of atomic and molecular structure and dynamics. *Annu. Rev. Phys. Chem.* **1982**, *33*, 223−255.
(9) McCurdy, C. W.; Lauderdale, J. G.; Mowrey, R. C. Complex self-consistent-field calculations on shape resonances in electron−Mg and electron−Ca scattering. *J. Chem. Phys.* **1981**, *75*, 1835−1842.
(10) Mishra, M.; Goscinski, O.; Öhrn, Y. Application of the second order dilated electron propagator to the treatment of Auger and shape resonances of Be. *J. Chem. Phys.* **1983**, *79*, 5505−5511.
(11) Mishra, M. K.; Venkatnathan, A. Treatment of shape and Auger resonances using the dilated electron propagator. *Int. J. Quantum Chem.* **2002**, *90*, 1334−1347.
(12) Sajeev, Y.; Mishra, M. K.; Vaval, N.; Pal, S. Fock space multireference coupled cluster calculations based on an underlying bivariational self-consistent field on Auger and shape resonances. *J. Chem. Phys.* **2004**, *120*, 67−72.
(13) Samanta, K.; Yeager, D. L. Investigation of ^{2}P Be^- shape resonances using a quadratically convergent complex multiconfigurational self-consistent field method. *J. Phys. Chem. B* **2008**, *112*, 16214−16219.
(14) Moiseyev, N.; Corcoran, C. Autoionizing states of H_2 and H_2^- using the complex-scaling method. *Phys. Rev. A* **1979**, *20*, 814.
(15) Jolicard, G.; Austin, E. J. Optical potential stabilisation method for predicting resonance levels. *Chem. Phys. Lett.* **1985**, *121*, 106−110.
(16) Jolicard, G.; Austin, E. J. Optical potential method of calculating resonance energies and widths. *Chem. Phys.* **1986**, *103*, 295−302.
(17) Riss, U.; Meyer, H.-D. Calculation of resonance energies and widths using the complex absorbing potential method. *J. Phys. B: At. Mol. Opt. Phys.* **1993**, *26*, 4503.
(18) Riss, U.; Meyer, H.-D. Reflection-free complex absorbing potentials. *J. Phys. B: At. Mol. Opt. Phys.* **1995**, *28*, 1475.
(19) Rom, N.; Lipkin, N.; Moiseyev, N. Optical potentials by the complex coordinate method. *Chem. Phys.* **1991**, *151*, 199−204.
(20) Karlsson, H. O. Accurate resonances and effective absorption of flux using smooth exterior scaling. *J. Chem. Phys.* **1998**, *109*, 9366−9371.
(21) Rom, N.; Engdahl, E.; Moiseyev, N. Tunneling rates in bound systems using smooth exterior complex scaling within the framework of the finite basis set approximation. *J. Chem. Phys.* **1990**, *93*, 3413−3419.
(22) Moiseyev, N. Derivations of universal exact complex absorption potentials by the generalized complex coordinate method. *J. Phys. B: At. Mol. Opt. Phys.* **1998**, *31*, 1431.

(23) Elander, N.; Yarevsky, E. Exterior complex scaling method applied to doubly excited states of helium. *Phys. Rev. A* **1998**, *57*, 3119.
(24) Telnov, D. A.; Chu, S.-I. Multiphoton detachment of H- near the one-photon threshold: Exterior complex-scaling−generalized pseudospectral method for complex quasienergy resonances. *Phys. Rev. A* **1999**, *59*, 2864.
(25) Kalita, D. J.; Gupta, A. K. Application of smooth exterior scaling method to study the time dependent dynamics of H_2^+ in intense laser field. *J. Chem. Phys.* **2010**, *133*, 134303.
(26) Kalita, D. J.; Gupta, A. K. Use of modified smooth exterior scaling method as an absorbing potential and its application. *J. Chem. Phys.* **2011**, *134*, 094301.
(27) Kalita, D. J.; Gupta, A. K. Application of smooth exterior scaling method to calculate the high harmonic generation spectra. *J. Chem. Phys.* **2013**, *138*, 074313.
(28) Mishra, M.; Froelich, P.; Öhrn, Y. The dilated electron propagator: a bi-orthogonal approach. *Chem. Phys. Lett.* **1981**, *81*, 339−346.
(29) Mishra, M.; Öhrn, Y.; Froelich, P. Self-consistent field theory of dilated atomic hamiltonians: Some remarks. *Phys. Lett. A* **1981**, *84*, 4−8.
(30) Mishra, M.; Kurtz, H. A.; Goscinski, O.; Öhrn, Y. Treatment of resonances with the dilated electron propagator: The ^{2}P shape resonance in e-Mg scattering. *J. Chem. Phys.* **1983**, *79*, 1896−1902.
(31) Mishra, M.; Goscinski, O.; Öhrn, Y. Numerical study of the bi-variational SCF method as a zeroth order dilated electron propagator. *J. Chem. Phys.* **1983**, *79*, 5494−5504.
(32) Yabushita, S.; McCurdy, C. W. Feshbach resonances in electron−molecule scattering by the complex multiconfiguration SCF and configuration interaction procedures: The $^1\Sigma_g^+$ autoionizing states of H_2. *J. Chem. Phys.* **1985**, *83*, 3547−3559.
(33) Honigmann, M.; Hirsch, G.; Buenker, R. J.; Petsalakis, I. D.; Theodorakopoulos, G. Complex coordinate calculations on auto-ionizing states of HeH and H_2. *Chem. Phys. Lett.* **1999**, *305*, 465−473.
(34) Medikeri, M. N.; Mishra, M. K. Lowest unoccupied molecular orbital as the resonant orbital. An investigation using the bi-variational self-consistent field method. *Chem. Phys. Lett.* **1995**, *246*, 26−32.
(35) Linderberg, J.; Öhrn, Y. *Propagators in Quantum Chemistry*; John Wiley & Sons, 2004.
(36) Venkatnathan, A.; Mahalakshmi, S.; Mishra, M. K. Higher order decouplings of the dilated electron propagator with applications to ^{2}P Be^-, ^{2}P Mg^- shape and ^{2}S $Be^+(1\ s^{-1})$ Auger resonances. *J. Chem. Phys.* **2001**, *114*, 35−47.
(37) Medikeri, M. N.; Mishra, M. K. Treatment of molecular resonances using the bi-orthogonal dilated electron propagator with application to the $^2\Pi_g$ shape resonance in e-N_2 scattering. *Int. J. Quantum Chem.* **1994**, *52*, 29−37.
(38) Medikeri, M. N.; Mishra, M. K. Characterization of molecular shape resonances using different decouplings of the dilated electron propagator with application to $^2\Pi$ CO^- and $^2B_{2g}$ $C2H_4^-$ shape resonances. *J. Chem. Phys.* **1995**, *103*, 676−682.
(39) Mahalakshmi, S.; Venkatnathan, A.; Mishra, M. K. Application of higher order decouplings of the dilated electron propagator to $^2\Pi$ CO^-, $^2\Pi_g$ $N_2^-$and $^2\Pi_g$ $C2H_2^-$ shape resonances. *J. Chem. Phys.* **2001**, *115*, 4549−4557.
(40) Moiseyev, N.; Hirschfelder, J. Representation of several complex coordinate methods by similarity transformation operators. *J. Chem. Phys.* **1988**, *88*, 1063−1065.
(41) Moiseyev, N.; Friedland, S.; Certain, P. R. Cusps, θ trajectories, and the complex virial theorem. *J. Chem. Phys.* **1981**, *74*, 4739−4740.
(42) Sajeev, Y.; Sindelka, M.; Moiseyev, N. Reflection-free complex absorbing potential for electronic structure calculations: Feshbach type autoionization resonance of Helium. *Chem. Phys.* **2006**, *329*, 307−312.
(43) Sajeev, Y.; Moiseyev, N. Reflection-free complex absorbing potential for electronic structure calculations: Feshbach-type auto-ionization resonances of molecules. *J. Chem. Phys.* **2007**, *127*, 034105.
(44) McCurdy, C. W.; Rescigno, T. N.; Davidson, E. R.; Lauderdale, J. G. Applicability of self-consistent field techniques based on the complex coordinate method to metastable electronic states. *J. Chem. Phys.* **1980**, *73*, 3268−3273.
(45) Berman, M.; Estrada, H.; Cederbaum, L. S.; Domcke, W. Nuclear dynamics in resonant electron-molecule scattering beyond the local approximation: The 2.3-eV shape resonance in N_2. *Phys. Rev. A* **1983**, *28*, 1363.
(46) Schneider, B. I.; Collins, L. A. Comparative study of low−energy $^2\Sigma_g^+$ and $^2\Pi_g$ scattering in molecular nitrogen. *Phys. Rev. A* **1984**, *30*, 95.
(47) Schneider, B.; Le Dourneuf, M.; Lan, V. K. Resonant vibrational excitation of N_2 by low-energy electrons: an ab initio R-matrix calculation. *Phys. Rev. Lett.* **1979**, *43*, 1926.
(48) Chao, J.-Y.; Falcetta, M.; Jordan, K. Application of the stabilization method to the $N_2^-(1^2\Pi g)$ and $Mg^-(1^2P)$ temporary anion states. *J. Chem. Phys.* **1990**, *93*, 1125−1135.
(49) Dubé, L.; Herzenberg, A. Absolute cross sections from the "boomerang model" for resonant electron-molecule scattering. *Phys. Rev. A* **1979**, *20*, 194.
(50) Rescigno, T.; Orel, A.; McCurdy, C. Application of complex coordinate SCF techniques to a molecular shape resonance: The $^2\Pi_g$ state of N_2^-. *J. Chem. Phys.* **1980**, *73*, 6347−6348.
(51) Donnelly, R. A. Coordinate-rotated propagator calculation on an N_2 shape resonance. *Int. J. Quantum Chem.* **1982**, *22*, 653−659.
(52) Sajeev, Y.; Santra, R.; Pal, S. Analytically continued Fock space multireference coupled-cluster theory: Application to the $^2\Pi_g$ shape resonance in e-N_2 scattering. *J. Chem. Phys.* **2005**, *122*, 234320.
(53) Zuev, D.; Jagau, T.-C.; Bravaya, K. B.; Epifanovsky, E.; Shao, Y.; Sundstrom, E.; Head-Gordon, M.; Krylov, A. I. Complex absorbing potentials within EOM-CC family of methods: Theory, implementation, and benchmarks. *J. Chem. Phys.* **2014**, *141*, 024102.
(54) Landau, A.; Moiseyev, N. Molecular resonances by removing complex absorbing potentials via Padé; application to CO^- and N_2^-. *J. Chem. Phys.* **2016**, *145*, 164111.
(55) White, A. F.; Epifanovsky, E.; McCurdy, C. W.; Head-Gordon, M. Second order Møller-Plesset and coupled cluster singles and doubles methods with complex basis functions for resonances in electron-molecule scattering. *J. Chem. Phys.* **2017**, *146*, 234107.
(56) Das, S.; Sajeev, Y.; Samanta, K. An Electron Propagator Approach Based on a Multiconfigurational Reference State for the Investigation of Negative-Ion Resonances Using a Complex Absorbing Potential Method. *J. Chem. Theory Comput.* **2020**, *16*, 5024−5034.
(57) Belogolova, A.; Dempwolff, A.; Dreuw, A.; Trofimov, A. A complex absorbing potential electron propagator approach to resonance states of metastable anions. *J. Phys.: Conf. Ser.* **2021**, *1847*, 012050.
(58) Das, S.; Samanta, K. Investigation of electron-induced scattering resonances using a multiconfigurational polarization propagator and a complex absorbing potential. *Chem. Phys.* **2023**, *564*, 111712.
(59) Ehrhardt, H.; Langhans, L.; Linder, F.; Taylor, H. Resonance scattering of slow electrons from H_2 and CO angular distributions. *Phys. Rev.* **1968**, *173*, 222.
(60) Zubek, M.; Szmytkowski, C. Calculation of resonant vibrational excitation of CO by scattering of electrons. *J. Phys. B: At. Mol. Phys.* **1977**, *10*, L27.
(61) Chandra, N. Low-energy electron scattering from CO. II. Ab initio study using the frame-transformation theory. *Phys. Rev. A* **1977**, *16*, 80.
(62) Donnelly, R. A. Second-order calculation on the doublet Pi CO shape resonance. *Int. J. Quantum Chem.* **1985**, *28*, 363−368.

https://doi.org/10.1021/acsomega.3c00033
ACS Omega 2023, 8, 7143−7150